UC Davis
UC Davis Previously Published Works

Title

Approximation of monotone clothoid segments by degree 7 Pythagorean–hodograph curves

Permalink

Authors

Farouki, Rida T
Pelosi, Francesca
Sampoli, Maria Lucia

Publication Date

DOI

Peer reviewed

Approximation of monotone clothoid segments by degree 7 Pythagorean-hodograph curves

Rida T. Farouki

Department of Mechanical and Aerospace Engineering,
University of California, Davis, CA 95616, USA.

Francesca Pelosi

Dipartimento di Matematica, Università di Roma "Tor Vergata,"
Via della Ricerca Scientifica, 00133 Roma, Italy.

Maria Lucia Sampoli

Dipartimento di Ingegneria dell'Informazione e
Scienze Matematiche, Università di Siena, San Niccolò,
Via Roma 56, 53100 Siena, Italy.

Abstract

The *clothoid* is a planar curve with the intuitive geometrical property of a linear variation of the curvature with arc length, a feature that is important in many geometric design applications. However, the exact parameterization of the clothoid is defined in terms of the irreducible *Fresnel integrals*, which are computationally expensive to evaluate and incompatible with the polynomial/rational representations employed in computer aided geometric design. Consequently, applications that seek to exploit the simple curvature variation of the clothoid must rely on approximations that satisfy a prescribed tolerance. In the present study, we investigate the use of planar Pythagorean–hodograph (PH) curves as polynomial approximants to monotone clothoid segments, based on geometric Hermite interpolation of end points, tangents, and curvatures, and precise matching of the clothoid segment arc length. The construction, employing PH curves of degree 7, involves iterative solution of a system of five algebraic equations in five real unknowns.

This is achieved by exploiting a closed–form solution to the problem of interpolating the specified data (except the curvatures) using quintic PH curves, to determine starting values that ensure rapid and accurate convergence to the desired solution.

e–mail: farouki@ucdavis.edu, pelosi@mat.uniroma2.it, marialucia.sampoli@unisi.it

1 Introduction

A plane curve with a prescribed initial point $\mathbf{p}_i$ and tangent orientation θ_i is uniquely determined by specifying its curvature κ as a function of the curve arc length s, measured from $\mathbf{p}_i$. The function $\kappa(s)$ is known as the *intrinsic equation* of the curve [27], and the simplest instances correspond to $\kappa(s) \equiv 0$ (straight lines) and $\kappa(s) \equiv$ a non–zero constant (circles).

The next–simplest instance, identified by a linear dependence of κ on s, defines a transcendental curve variously known as the *clothoid*, *Euler spiral*, or *Cornu spiral*. We may elucidate the nature of this curve as follows. Setting $\kappa = \mathrm{d}\theta/\mathrm{d}s$ (where θ is the tangent orientation) and $\kappa(s) = c\,s + \kappa_i$ for some constant c and initial curvature κ_i at $s = 0$, we have

$$\frac{\mathrm{d}\theta}{\mathrm{d}s} = c\,s + \kappa_i\,,$$

and on integration with an initial tangent orientation θ_i, we obtain

$$\theta(s) = \tfrac{1}{2}c\,s^2 + \kappa_i s + \theta_i\,.$$

Moreover, since

$$\frac{\mathrm{d}x}{\mathrm{d}s} = \cos\theta(s)\,, \quad \frac{\mathrm{d}y}{\mathrm{d}s} = \sin\theta(s)\,,$$

a further integration with initial point $\mathbf{p}_i = (x_i, y_i)$ yields the curve $\mathbf{c}(s) = (x(s), y(s))$ defined by

$$x(s) = x_i + \int_0^s \cos(\tfrac{1}{2}c\,t^2 + \kappa_i t + \theta_i)\,\mathrm{d}t\,,$$

$$y(s) = y_i + \int_0^s \sin(\tfrac{1}{2}c\,t^2 + \kappa_i t + \theta_i)\,\mathrm{d}t\,. \tag{1}$$

In canonical form with $(x_i, y_i) = (0, 0)$, $\theta_i = \kappa_i = 0$, and $c = \pi$, we obtain the *Fresnel integrals*

$$C(s) := \int_0^s \cos(\tfrac{1}{2}\pi t^2)\,\mathrm{d}t\,, \quad S(s) := \int_0^s \sin(\tfrac{1}{2}\pi t^2)\,\mathrm{d}t\,, \tag{2}$$

in (1) — as illustrated in Figure 1. Since we have $\mathbf{c}'(s) = (\cos\tfrac{1}{2}\pi s^2, \sin\tfrac{1}{2}\pi s^2)$ and $\mathbf{c}''(s) = \pi s(-\sin\tfrac{1}{2}\pi s^2, \cos\tfrac{1}{2}\pi s^2)$ the parametric speed and curvature are

$\sigma(s) = 1$ and $\kappa(s) = \pi s$. Thus, any clothoid segment $s \in [\, s_i, s_f \,]$ admits the simple expression

$$E \;=\; \int_{s_i}^{s_f} \kappa^2(s) \, \mathrm{d}s \;=\; \frac{\pi^2}{3}(s_f^3 - s_i^3)$$

for the *bending energy* integral (i.e., the energy stored in an initially–straight thin elastic beam that is bent to assume the shape of the clothoid segement). Moreover, the energy per unit length is $E/(s_f - s_i) = s_i^2 + s_i s_f + s_f^2$.

As evident in Figure 1, the point $\mathbf{c}(0)$ is an inflection at the origin, with $\kappa = 0$, and the curve spirals infinitely many times about the points $(\pm\frac{1}{2}, \pm\frac{1}{2})$ while the curvature increases with arc length s at the constant rate π.
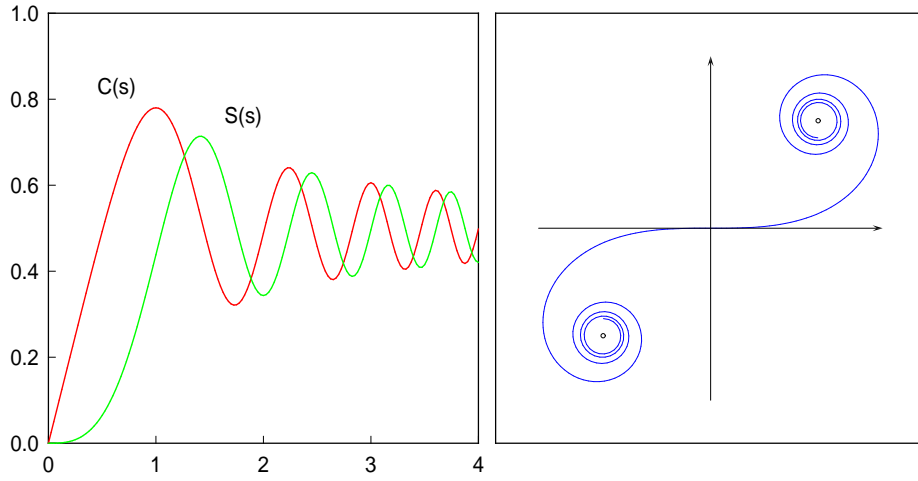

Figure 1: Left: the Fresnel integrals (2) for $0 \leq s \leq 4$. Right: the clothoid defined by (2) with $x_i = y_i = \theta_i = \kappa_i = 0$ and $c = \pi$ has the linear intrinsic equation $\kappa(s) = \pi s$. The curve has the limit points $(\pm\frac{1}{2}, \pm\frac{1}{2})$ as $s \to \pm\infty$.

The winding nature of the curve defined by (1)–(2) led the mathematician Ernesto Cesàro to coin the name "clothoid" after *Clotho*, one of the daughters of Zeus and Themis, known as the Moirai (or " Fates") in Greek mythology. Clotho (the *spinner*) spun the thread of life onto a spindle, while her sisters Lachesis (the *apportioner*) and Atropos (the *inevitable*) measured and cut it, determining the life span and the moment of death of each mortal.

This study focuses on *geometrical* approximation of finite clothoid curve segments, rather than approximation of the Fresnel integrals (2) individually.

A distinctive feature of the proposed approach is to exactly match *arc lengths* of clothoid segments between points at which discrete geometrical properties (points, tangents, curvatures) of the clothoid are interpolated.[1] We focus, in particular, on *monotone* clothoid segments along which the x, y coordinates are increasing or decreasing. Such segments (or subsegments thereof) are of primary interest in applications, and the restriction to monotone segments also ensures a higher approximation accuracy. Greater extents of the clothoid can be represented by G^2 concatenations of such segments.

Because of their monotone curvature variation, clothoid segments are of interest in diverse applications, including the design of highways and railways; path planning for mobile robots; specification of bipedal locomotion; control of unmanned aerial vehicles and autonomous ground vehicles; and smoothing of CNC machining toolpaths [4, 21, 24, 28, 30, 31, 37, 38, 39, 41, 42, 44]. We are interested here in approximating canonical–form clothoid segments using *Pythagorean–hodograph* (PH) *curves* [13]. A distinct advantage of PH curves is their polynomial parametric speed and arc length, and rational curvature, which allow the approximation problem to be formulated as the solution of a system of polynomial equations, yielding approximants in standard Bézier form. We do not discuss here the application of translation/rotation/scaling transformations to canonical–form clothoid segments to suit the requirements of specific applications, since this is addressed elsewhere [3, 6, 29, 30, 31].

There have been several prior approaches to the approximation of clothoid segments by more tractable curve forms. In [40] polynomial approximations to clothoid segments are constructed as Hermite interpolants of odd degree n to end points and derivatives up to order $\frac{1}{2}(n-1)$. The use of arc (piecewise–circular) splines was proposed in [32, 36]: these approximants have piecewise–constant curvature, and they are only G^1 continuous. The study [7] describes a scheme to approximate clothoid segments by quintic Bézier curves, based on adaptive sampling and look–up tables, and the approach proposed in [6] employs storage of discrete points of the canonical–form clothoid in a look-up table, with intermediate points computed by circular interpolation. A unique feature of PH curves is the ability to reproduce a *global* property of clothoid segments — the *exact* segment arc length. Moreover, PH curve approximants are found to closely mimic the clothoid arc–length parameterization.

---

[1] A single clothoid segment of given arc length cannot, in general, match prescribed end points, tangents, and curvatures [5]. The focus herein is to approximate a given clothoid segment, not to construct a clothoid segment from specified G^2 end–point data.

3

A number of related studies [12, 16, 19, 22, 23, 47, 48] have been concerned with designing "transition" curves between elementary (linear/circular) path segments. However, the focus in these studies has been on the smoothness or curvature monotonicity of the transition curve, without explicitly attempting to achieve a linear dependence of curvature on arc length.

The remainder of this paper is structured as follows. Section 2 describes a methodology to accurately compute the (x, y) coordinates of clothoid points corresponding to a specified arc length s, a basic requirement in assessing the quality of approximants to clothoid segments. Sections 3 and 4 then review the basic features of planar Pythagorean–hodograph (PH) curves, and discuss their use in approximating finite clothoid segments. Section 5 elaborates on these principles in the specific context of degree 7 PH curves, and formulates a system of equations that characterizes PH curves matching the end points, tangents, and curvatures, and the total arc length, of a prescribed clothoid segment. The methodology for determining the solutions of this system of equations is illustrated by a selection of computed examples in Section 6. Finally, in Section 7 we summarize the key contributions of the present study, and identify possible aspects for further investigation.

2 Computation of clothoid points

To assess the accuracy of parametric polynomial approximations to clothoid segments, it is necessary to have the ability to compute the integrals (2) for any s to a prescribed accuracy. Several authors [1, 2, 25, 33, 34, 45, 46] have proposed numerical methods for evaluation of the Fresnel integrals. Although some of these methods are capable of high accuracy, they are not compatible with the polynomial or rational Bézier/B–spline representations employed in computer–aided geometric design, which key functions (computation of curve intersections, construction of offset curves, etc.) depend upon.

A *turning point* of the clothoid is identified as a location where the tangent is horizontal or vertical. Such points occur where $\frac{1}{2}\pi s^2$ is an integer multiple k of $\frac{1}{2}\pi$ — i.e., when $s = s_k$, where

$$s_k := \sqrt{k}, \quad k = 0, 1, 2, \ldots$$

The turning points delineate *monotone clothoid segments* along which x and y are increasing or decreasing. We denote by C_k the k–th monotone segment,

4

defined on $s \in [\,s_{k-1}, s_k\,]$. It has arc length $\Delta s_k = s_k - s_{k-1}$, tangent turning angle $\Delta \theta_k = \frac{1}{2}\pi$, and initial/final curvatures $\kappa_i = \pi\sqrt{k-1}$, $\kappa_f = \pi\sqrt{k}$.

To approximate any monotone clothoid segment, the coordinates of the two turning points that delineate it must be computed to high accuracy. To accomplish this, we employ the algorithm proposed[2] by Alazah et al. [1]. For $n = 1, 2, 3, \ldots$ a sequence of complex–valued functions are defined by

$$\mathbf{F}_n(x) \;=\; \frac{1}{\exp(2\,\mathbf{a}_n x) + 1} \;+\; \frac{x\,\exp(\mathrm{i}\,x^2)}{\mathbf{a}_n} \sum_{k=1}^{n} \frac{\exp(-u_k)}{x^2 + \mathrm{i}\,u_k}\,,$$

where

$$\mathbf{a}_n \;=\; \sqrt{(n+\tfrac{1}{2})\pi}\,\exp(-\mathrm{i}\tfrac{1}{4}\pi)\,, \quad u_k \;=\; \frac{(k-\tfrac{1}{2})^2\,\pi}{n+\tfrac{1}{2}}\,.$$

For increasing n, these functions determine a sequence of rapidly converging approximations to the Fresnel integrals (2) through the expressions

$$\begin{aligned}
C_n(s) &= \tfrac{1}{2} - \mathrm{Re}[\,\mathbf{F}_n(x)\,] + \mathrm{Im}[\,\mathbf{F}_n(x)\,]\,, \\
S_n(s) &= \tfrac{1}{2} - \mathrm{Re}[\,\mathbf{F}_n(x)\,] - \mathrm{Im}[\,\mathbf{F}_n(x)\,]\,,
\end{aligned}$$

where we set $x = \sqrt{\tfrac{1}{2}\pi}\,s$.

The coordinates of the first twelve turning points, computed using the above scheme with $n = 16$, are listed to 12 decimal places below:

$$\begin{aligned}
\mathbf{c}_1 &= (0.779893400377, 0.438259147390)\,, \\
\mathbf{c}_2 &= (0.528891595111, 0.713972214022)\,, \\
\mathbf{c}_3 &= (0.321056186411, 0.517305121864)\,, \\
\mathbf{c}_4 &= (0.488253406075, 0.343415678364)\,, \\
\mathbf{c}_5 &= (0.640806840445, 0.491392538968)\,, \\
\mathbf{c}_6 &= (0.506641564063, 0.628939658540)\,, \\
\mathbf{c}_7 &= (0.380390693768, 0.505318740045)\,, \\
\mathbf{c}_8 &= (0.495619698096, 0.387968992637)\,, \\
\mathbf{c}_9 &= (0.605720789298, 0.496312998967)\,, \\
\mathbf{c}_{10} &= (0.503158104723, 0.600362387251)\,, \\
\mathbf{c}_{11} &= (0.404260497245, 0.502743998716)\,, \\
\mathbf{c}_{12} &= (0.497587274289, 0.408301331932)\,.
\end{aligned}$$

---

[2]The notation employed here is a simplified form of that in [1].

As a further check on their accuracy, these points were also computed using a composite Simpson quadrature rule [9], and were found to be in agreement with the above values to the 12 decimal places indicated.

3   Planar Pythagorean-hodograph curves

Since the clothoid is a transcendental curve, it is impossible to parameterize any segment of it exactly by polynomial or rational functions. Consequently, we investigate here the problem of accurately approximating finite segments of the clothoid by Pythagorean–hodograph (PH) curves [13]. A Weierstrass–type theorem for Pythagorean–hodograph curves [8] establishes their ability to uniformly approximate any given C^1 curve.

In the complex representation [11], a planar PH curve is constructed from a complex polynomial $\mathbf{w}(\xi) = u(\xi) + \mathrm{i}\,v(\xi)$ by integrating the expression

$$\mathbf{r}'(\xi) \;=\; \mathbf{w}^2(\xi)\,. \tag{3}$$

If $\mathbf{w}(\xi)$ is of degree m, it may be defined by its complex Bernstein coefficients $\mathbf{w}_0, \ldots, \mathbf{w}_m$ as

$$\mathbf{w}(\xi) \;=\; \sum_{k=0}^{m} \mathbf{w}_k\, b_k^m(\xi)\,, \quad b_k^m(\xi) \;=\; \binom{m}{k}(1-\xi)^{m-k}\xi^k\,. \tag{4}$$

Integrating (3) yields a planar PH curve of degree $n = 2m+1$. The expression (3) can be written as

$$\mathbf{r}'(\xi) \;=\; \sum_{k=0}^{2m} \mathbf{q}_k\, b_k^{2m}(\xi)\,,$$

with coefficients given by

$$\mathbf{q}_k \;=\; \sum_{j=\max(0,k-m)}^{\min(m,k)} \frac{\dbinom{m}{j}\dbinom{m}{k-j}}{\dbinom{2m}{k}}\,\mathbf{w}_j\mathbf{w}_{k-j}\,, \quad k = 0,\ldots,2m\,. \tag{5}$$

Integration of (3) with $\mathbf{r}(0) = \mathbf{p}_0$ then gives the remaining control points $\mathbf{p}_k$ in the Bézier representation

$$\mathbf{r}(\xi) \;=\; \sum_{k=0}^{n} \mathbf{p}_k b_k^n(\xi) \tag{6}$$

6

of the PH curve, through the formulae

$$\mathbf{p}_k = \mathbf{p}_{k-1} + \frac{1}{n}\mathbf{q}_{k-1}, \quad k = 1, \ldots, n. \tag{7}$$

The *parametric speed* of $\mathbf{r}(\xi)$, which specifies the derivative $\mathrm{d}s/\mathrm{d}\xi$ of the arc length s with respect to the curve parameter ξ, is specified by

$$\sigma(\xi) = |\mathbf{r}'(\xi)| = |\mathbf{w}(\xi)|^2. \tag{8}$$

Expressing the parametric speed in Bernstein form as

$$\sigma(\xi) = \sum_{k=0}^{2m} \sigma_k \, b_k^{2m}(\xi),$$

it has the (real) coefficients

$$\sigma_k = \sum_{j=\max(0,k-m)}^{\min(m,k)} \frac{\binom{m}{j}\binom{m}{k-j}}{\binom{2m}{k}} \mathbf{w}_j \overline{\mathbf{w}}_{k-j}, \quad k = 0, \ldots, 2m. \tag{9}$$

The cumulative arc length function, obtained by integration of $\sigma(\xi)$, is the degree n polynomial

$$s(\xi) = \sum_{k=0}^{n} s_k \, b_k^n(\xi), \tag{10}$$

with coefficients

$$s_0 = 0 \quad \text{and} \quad s_k = s_{k-1} + \frac{1}{n}\sigma_{k-1}, \quad k = 1, \ldots, n, \tag{11}$$

and the total arc length is

$$S = \int_0^1 \sigma(\xi)\,\mathrm{d}\xi = \frac{1}{n}\sum_{k=0}^{2m}\sigma_k = s_n.$$

Using (3), the tangent and curvature of $\mathbf{r}(\xi)$ may be expressed as

$$\mathbf{t}(\xi) = \frac{\mathbf{r}'(\xi)}{|\mathbf{r}'(\xi)|} = \frac{\mathbf{w}^2(\xi)}{|\mathbf{w}(\xi)|^2} = \mathbf{w}(\xi)/\overline{\mathbf{w}}(\xi), \tag{12}$$

7

$$\kappa(\xi) \;=\; \frac{(\mathbf{r}'(\xi) \times \mathbf{r}''(\xi)) \cdot \mathbf{k}}{|\mathbf{r}'(\xi)|^3} \;=\; 2\,\frac{\mathrm{Im}(\overline{\mathbf{w}}(\xi)\mathbf{w}'(\xi))}{|\mathbf{w}(\xi)|^4}\,, \tag{13}$$

where $\mathbf{k}$ is a unit vector orthogonal to the plane of $\mathbf{r}(\xi)$. Setting

$$\mathbf{z}(\xi) \;=\; \ln \mathbf{w}(\xi) \;=\; \ln|\mathbf{w}(\xi)| + \mathrm{i}\arg(\mathbf{w}(\xi))\,, \tag{14}$$

we have $\mathbf{z}'(\xi) = \mathbf{w}'(\xi)/\mathbf{w}(\xi)$ and this gives the more compact expression

$$\kappa(\xi) \;=\; \frac{2}{\sigma(\xi)}\,\mathrm{Im}(\mathbf{z}'(\xi))\,.$$

Noting that $\sigma' = 2\,\mathrm{Re}(\overline{\mathbf{w}}\mathbf{w}')$ and $\mathrm{Im}(\mathbf{z}') = 2\,\mathrm{Im}(\overline{\mathbf{w}}\mathbf{w}')/\sigma$, we can express the arc–length derivative of curvature as

$$\frac{\mathrm{d}\kappa}{\mathrm{d}s} \;=\; \frac{1}{\sigma}\frac{\mathrm{d}\kappa}{\mathrm{d}\xi} \;=\; \frac{2}{\sigma^2(\xi)}\mathrm{Im}(\mathbf{z}''(\xi) - \mathbf{z}'^2(\xi))\,, \tag{15}$$

where

$$\mathbf{z}'(\xi) \;=\; \frac{\mathbf{w}'(\xi)}{\mathbf{w}(\xi)}\,, \quad \mathbf{z}''(\xi) \;=\; \frac{\mathbf{w}(\xi)\mathbf{w}''(\xi) - \mathbf{w}'^2(\xi)}{\mathbf{w}^2(\xi)}\,. \tag{16}$$

4   Formulation of approximants

Consider the approximation of a segment $s \in [\,s_i, s_f\,]$ of the canonical–form clothoid $\mathbf{c}(s) = (C(s), S(s))$ specified by the Fresnel integrals (2), by a planar PH curve $\mathbf{r}(\xi)$, $\xi \in [\,0, 1\,]$ generated through (3) by the complex polynomial (4), with parametric speed (8), arc length function (10), and curvature (13). We focus here on G^2 approximations to clothoid segments with turning angles not exceeding $\frac{1}{2}\pi$ (typically, monotone segments). Approximants of greater extent can be constructed by concatenating these segments (or subsegments thereof) to obtain extended G^2 piecewise PH approximants.

Although $\mathbf{r}(\xi)$ employs a general parameter ξ, there is a simple procedural relationship between this parameter and arc length on a PH curve. Namely, the parameter value ξ_* corresponding to arc length s_* (measured from $\xi = 0$) along $\mathbf{r}(\xi)$ is the unique real root of the polynomial equation

$$s(\xi_*) \;=\; s_*\,, \tag{17}$$

where $s(\xi)$ is the arc length function defined by (10) and (11). The uniqueness of this root is ensured by the fact that, since $s(\xi)$ is the integral of the non–negative parametric speed $\sigma(\xi)$, it is a monotone–increasing polynomial. This property is of great importance in real–time motion control [17, 20, 43].

8

In general, it is desirable that the approximant satisfy certain boundary conditions. First, writing[3] $\Delta\mathbf{p} = \Delta x + \mathrm{i}\,\Delta y = \mathbf{c}(s_f) - \mathbf{c}(s_i)$ and $\Delta s = s_f - s_i$, and requiring the approximant to match the end points and total arc length of the clothoid segment yields the conditions

$$\frac{\mathbf{q}_0 + \cdots + \mathbf{q}_{2m}}{n} = \Delta\mathbf{p} \quad \text{and} \quad \frac{\sigma_0 + \cdots + \sigma_{2m}}{n} = \Delta s\,, \qquad (18)$$

with $\mathbf{q}_0, \ldots, \mathbf{q}_{2m}$ and $\sigma_0, \ldots, \sigma_{2m}$ given in terms of $\mathbf{w}_0, \ldots, \mathbf{w}_m$ by (5) and (9). Furthermore, matching the initial and final tangents of the clothoid segment yields the equations

$$\arg(\mathbf{w}_0/\overline{\mathbf{w}}_0) = 2\,\arg(\mathbf{w}_0) = \tfrac{1}{2}\pi s_i^2\,,$$

$$\arg(\mathbf{w}_m/\overline{\mathbf{w}}_m) = 2\,\arg(\mathbf{w}_m) = \tfrac{1}{2}\pi s_f^2\,, \qquad (19)$$

and matching the initial and final curvatures yields

$$2\,m\,\mathrm{Im}(\overline{\mathbf{w}}_0\mathbf{w}_1) = \pi s_i|\mathbf{w}_0|^4\,, \quad 2\,m\,\mathrm{Im}(\overline{\mathbf{w}}_{m-1}\mathbf{w}_m) = \pi s_f|\mathbf{w}_m|^4\,. \qquad (20)$$

The system of equations (18)–(20) specify 7 scalar constraints on the $2(m+1)$ degrees of freedom in $\mathbf{w}_0, \ldots, \mathbf{w}_m$ that identify PH curve interpolants to planar G^2 data with prescribed arc lengths. Clearly, PH curves of degree $n \geq 7$ (i.e., $m \geq 3$) will be required to satisfy all of these conditions.

Now if $\mathbf{w}(\xi) = u(\xi) + \mathrm{i}\,v(\xi)$ has the complex coefficients $\mathbf{w}_k = u_k + \mathrm{i}\,v_k$, $k = 0, \ldots, m$ we have $x'(\xi) = u^2(\xi) - v^2(\xi)$, $y'(\xi) = 2\,u(\xi)v(\xi)$, and $\sigma(\xi) = s'(\xi) = u^2(\xi) + v^2(\xi)$, where $u(\xi)$ and $v(\xi)$ have coefficients $u_0, \ldots, u_m$ and $v_0, \ldots, v_m$. Hence, to match the displacement $\Delta\mathbf{p} = \Delta x + \mathrm{i}\,\Delta y$ and arc length Δs, we must have

$$\int_0^1 u^2(\xi) - v^2(\xi)\,\mathrm{d}\xi = \Delta x\,, \quad \int_0^1 2\,u(\xi)v(\xi)\,\mathrm{d}\xi = \Delta y\,,$$

$$\int_0^\xi u^2(\xi) + v^2(\xi)\,\mathrm{d}\xi = \Delta s\,.$$

These conditions are equivalent to the simpler system of equations

$$\int_0^1 u^2(\xi)\,\mathrm{d}\xi = \tfrac{1}{2}(\Delta s + \Delta x)\,, \quad \int_0^1 v^2(\xi)\,\mathrm{d}\xi = \tfrac{1}{2}(\Delta s - \Delta x)\,, \qquad (21)$$

[3]Note that $\mathbf{c}(s_i)$, $\mathbf{c}(s_f)$ must be determined numerically from the Fresnel integrals (2).

9

$$\int_0^1 u(\xi)v(\xi)\,\mathrm{d}\xi \;=\; \tfrac{1}{2}\Delta y\,, \tag{22}$$

which are quadratic in the Bernstein coefficients of $u(\xi)$ and $v(\xi)$. For brevity, we now set

$$(\alpha_i, \beta_i) \;=\; (\cos\tfrac{1}{4}\pi s_i^2, \sin\tfrac{1}{4}\pi s_i^2)\,, \quad (\alpha_f, \beta_f) \;=\; (\cos\tfrac{1}{4}\pi s_f^2, \sin\tfrac{1}{4}\pi s_f^2)\,. \tag{23}$$

The end–tangent conditions (19) then give

$$(u_0, v_0) \;=\; \sqrt{\lambda_0}\,(\alpha_i, \beta_i)\,, \quad (u_m, v_m) \;=\; \sqrt{\lambda_m}\,(\alpha_f, \beta_f)\,, \tag{24}$$

where $\lambda_0 = |\mathbf{w}_0|^2$, $\lambda_m = |\mathbf{w}_m|^2$ are positive free parameters, while the end–curvature conditions (20) become

$$\alpha_i v_1 - \beta_i u_1 \;=\; \frac{\pi s_i \lambda_0^{3/2}}{2\,m}\,, \quad \beta_f u_{m-1} - \alpha_f v_{m-1} \;=\; \frac{\pi s_f \lambda_m^{3/2}}{2\,m}\,. \tag{25}$$

Equations (24) replace the pairs (u_0, v_0) and (u_m, v_m) by the single unknowns λ_0 and λ_m. Also, equations (25) may be regarded as determining v_1 and v_{m-1} in terms of u_1 and u_{m-1} (or vice–versa). We then have the remaining $2m-2$ free variables $u_1, \ldots, u_{m-1}, v_2, \ldots, v_{m-2}, \lambda_0, \lambda_m$ which must satisfy the three quadratic constraints defined by equations (21)–(22). This is possible only if $m \geq 3$, in which case we have $2m-5$ residual free variables.

5   Degree 7 PH curve approximants

A method for constructing degree 7 planar PH curves that match prescribed initial/final points, parametric derivatives, and curvatures was described in [26] and it was observed that there are, in general, eight possible solutions.

In the present context, we substitute unit end tangents for the parametric derivatives, and exploit the resulting degrees of freedom to impose conditions appropriate to the approximation of clothoid segments, namely (1) specifying the arc length of the interpolant, and (2) imposition of equal–magnitude end derivatives. Although this problem also has multiple solutions, a scheme for identifying accurate approximations to the "good" solution allows it to be computed to machine precision by rapidly–convergent iterative methods.

In the case of degree 7 PH curves ($m = 3$), equations (21)–(22) become

$$10\,u_0^2 + 6\,u_1^2 + 6\,u_2^2 + 10\,u_3^2 + 10\,(u_0 u_1 + u_2 u_3)$$
$$+\ 9\,u_1 u_2 + 4\,(u_0 u_2 + u_1 u_3) + u_0 u_3 \ =\ 35\,(\Delta s + \Delta x)\,, \tag{26}$$

$$10\,v_0^2 + 6\,v_1^2 + 6\,v_2^2 + 10\,v_3^2 + 10\,(v_0 v_1 + v_2 v_3)$$
$$+\ 9\,v_1 v_2 + 4\,(v_0 v_2 + v_1 v_3) + v_0 v_3 \ =\ 35\,(\Delta s - \Delta x)\,, \tag{27}$$

$$20\,u_0 v_0 + 12\,u_1 v_1 + 12\,u_2 v_2 + 20\,u_3 v_3$$
$$+\ 10\,(u_0 v_1 + u_1 v_0) + 10\,(u_2 v_3 + u_3 v_2) + 9\,(u_1 v_2 + u_2 v_1)$$
$$+\ 4\,(u_0 v_2 + u_2 v_0) + 4\,(u_1 v_3 + u_3 v_1) + u_0 v_3 + u_3 v_0 \ =\ 70\,\Delta y\,. \tag{28}$$

Together with (25), and (u_0, v_0) and (u_3, v_3) given by (24) with $m = 3$, we have a system of five equations in the six unknowns $\lambda_0, \lambda_3, u_1, v_1, u_2, v_2$.

To simplify the analysis, we eliminate the additional degree of freedom by choosing $\lambda_0 = \lambda_3 = \lambda$. Since $|\mathbf{r}'(0)| = \lambda_0$ and $|\mathbf{r}'(1)| = \lambda_3$, this assumption is consistent with the constant parametric speed of the clothoid defined by (2).

Proposition 1. *The degree 7 PH curve approximant to the monotone clothoid segment C_i, with end–point displacement $\Delta x = x_i - x_{i-1}$, $\Delta y = y_i - y_{i-1}$, and total arc length $\Delta s = s_i - s_{i-1}$, is identified by a solution to the following system of five equations*

$$\alpha_i q_1 - \beta_i p_1 \ =\ \frac{\pi s_i}{6}\lambda\,, \quad \beta_f p_2 - \alpha_f q_2 \ =\ \frac{\pi s_f}{6}\lambda\,, \tag{29}$$

$$[\,10\,\alpha_i^2 + 6\,p_1^2 + 6\,p_2^2 + 10\,\alpha_f^2 + 10\,(\alpha_i p_1 + \alpha_f p_2)$$
$$+\ 9\,p_1 p_2 + 4\,(\alpha_i p_2 + \alpha_f p_1) + \alpha_i \alpha_f\,]\,\lambda \ =\ 35(\Delta s + \Delta x)\,, \tag{30}$$

$$[\,10\,\beta_i^2 + 6\,q_1^2 + 6\,q_2^2 + 10\,\beta_f^2 + 10\,(\beta_i q_1 + \beta_f q_2)$$
$$+\ 9\,q_1 q_2 + 4\,(\beta_i q_2 + \beta_f q_1) + \beta_i \beta_f\,]\,\lambda \ =\ 35(\Delta s - \Delta x)\,, \tag{31}$$

$$[\,20\,\alpha_i \beta_i + 12\,p_1 q_1 + 12\,p_2 q_2 + 20\,\alpha_f \beta_f$$
$$+\ 10\,(\alpha_i q_1 + \beta_i p_1) + 10\,(\beta_f p_2 + \alpha_f q_2) + 9\,(p_1 q_2 + p_2 q_1)$$
$$+\ 4\,(\alpha_i q_2 + \beta_i p_2) + 4\,(\beta_f p_1 + \alpha_f q_1) + \alpha_i \beta_f + \alpha_f \beta_i\,]\,\lambda \ =\ 70\,\Delta y\,. \tag{32}$$

in the real variables $\lambda, p_1, q_1, p_2, q_2$ where $\lambda > 0$ and α_i, β_i are defined by (23).

11

Proof : The values (23) ensure the correct clothoid segment end tangents, and on setting

$$(u_1, v_1) \; = \; \sqrt{\lambda}\,(p_1, q_1)\,, \quad (u_2, v_2) \; = \; \sqrt{\lambda}\,(p_2, q_2) \tag{33}$$

in (24), the equations (25) with $m = 3$, that ensure satisfaction of the end curvatures, reduce to (29). Finally, substituting from (24), we can re–write equations (26)–(28), ensuring satisfaction of the clothoid segment end points and total arc length, in the form (30)–(32). ∎

Equations (29)–(32) are linear in λ and at most quadratic in p_1, q_1, p_2, q_2. As usual with the construction of PH curves that interpolate discrete data, this system may admit multiple solutions, among which the "good" solution (closely approximating the clothoid segment) must be identified [18, 26, 35].

Now the parameter λ must evidently be positive to guarantee polynomials $u(\xi), v(\xi) \in \mathbb{R}[\xi]$ as the real and imaginary parts of the complex polynomial $\mathbf{w}(\xi) = u(\xi) + \mathrm{i}\,v(\xi)$. However, as we now show, there is an upper bound on the λ values that admit real solutions of the system (29)–(32).

Proposition 2. *For the system of equations* (29)–(32) *to have real solutions, the positive parameter* λ *must satisfy*

$$\lambda \; < \; \lambda_{\max} \; := \; \min\left(\frac{15\,(\Delta s + \Delta x)}{2\,\alpha_i^2 + \alpha_i \alpha_f + 2\,\alpha_f^2}, \frac{15\,(\Delta s - \Delta x)}{2\,\beta_i^2 + \beta_i \beta_f + 2\,\beta_f^2} \right)\,. \tag{34}$$

Proof : For a specified λ, equations (30) and (31) define conic curves in the (p_1, p_2) and (q_1, q_2) planes, while equation (32) defines a quadric surface in $\mathbb{R}^4$ spanned by the coordinates (p_1, p_2, q_1, q_2). Introducing the new coordinates (u_1, u_2) and (v_1, v_2) defined by

$$p_1 \; = \; \sqrt{2}\,(u_1 + u_2) - \frac{(4\,\alpha_i - 2\,\alpha_f)}{3}\,, \quad p_2 \; = \; \sqrt{2}\,(u_2 - u_1) - \frac{(4\,\alpha_f - 2\,\alpha_i)}{3}\,,$$

$$q_1 \; = \; \sqrt{2}\,(v_1 + v_2) - \frac{(4\,\beta_i - 2\,\beta_f)}{3}\,, \quad q_2 \; = \; \sqrt{2}\,(v_2 - v_1) - \frac{(4\,\beta_f - 2\,\beta_i)}{3}\,,$$

equations (30) and (31) can be reduced to

$$\frac{u_1^2}{7} + u_2^2 \; = \; \gamma\,, \qquad \frac{v_1^2}{7} + v_2^2 \; = \; \delta\,, \tag{35}$$

12

where

$$\gamma = \frac{5\,(\Delta s + \Delta x)}{6\,\lambda} - \frac{(2\,\alpha_i^2 + \alpha_i\alpha_f + 2\,\alpha_f^2)}{18}\,, \tag{36}$$

$$\delta = \frac{5\,(\Delta s - \Delta x)}{6\,\lambda} - \frac{(2\,\beta_i^2 + \beta_i\beta_f + 2\,\beta_f^2)}{18}\,. \tag{37}$$

In order for both these conics to have non–null real loci, we must have $\gamma > 0$ and $\delta > 0$, which is equivalent to the condition that λ satisfies (34). ∎

When (34) is satisfied, p_1, p_2 and q_1, q_2 may be parameterized in terms of angular variables ϕ and ψ as

$$p_1(\phi) = \sqrt{2\gamma}\,(\sqrt{7}\cos\phi + \sin\phi) - \frac{4\,\alpha_i - 2\,\alpha_f}{3}\,,$$

$$p_2(\phi) = \sqrt{2\gamma}\,(\sin\phi - \sqrt{7}\cos\phi) - \frac{4\,\alpha_f - 2\,\alpha_i}{3}\,,$$

$$q_1(\psi) = \sqrt{2\,\delta}\,(\sqrt{7}\cos\psi + \sin\psi) - \frac{4\,\beta_i - 2\,\beta_f}{3}\,,$$

$$q_2(\psi) = \sqrt{2\,\delta}\,(\sin\psi - \sqrt{7}\cos\psi) - \frac{4\,\beta_f - 2\,\beta_i}{3}\,,$$

where γ and δ depend on λ as in (36)–(37). On substituting into (29)–(32), the construction is reduced to computing the solutions of three equations in the variables λ, ϕ, ψ. However, these equations are of greater complexity, and a simpler dimensional reduction can be obtained as follows.

Remark 1. By means of equations (29), the variables p_1, q_1 and p_2, q_2 may be expressed in terms of λ and real parameters τ_1 and τ_2 as

$$p_1(\tau_1) = \alpha_i\tau_1 - \beta_i\frac{\pi s_i}{6}\lambda\,, \quad q_1(\tau_1) = \beta_i\tau_1 + \alpha_i\frac{\pi s_i}{6}\lambda\,, \tag{38}$$

$$p_2(\tau_2) = -\alpha_f\tau_2 + \beta_f\frac{\pi s_f}{6}\lambda\,, \quad q_2(\tau_2) = -\beta_f\tau_2 - \alpha_f\frac{\pi s_f}{6}\lambda\,, \tag{39}$$

and substituting these expressions in (30)–(32) yields three equations in three real variables, that are cubic in λ and quadratic in τ_1, τ_2. Upon solving these equations, the values of p_1, q_1 and p_2, q_2 may be obtained by substituting the solutions λ, τ_1, τ_2 in (38) and (39).

13

To obtain a starting approximation for the good solution $\lambda, p_1, q_1, p_2, q_2$ of equations (29)–(32), we invoke the procedure described in [14] to compute the quintic PH curve with equal–magnitude end derivatives, having the same end points, end tangents, and arc length Δs as the clothoid segment.[4] We then degree–elevate the quadratic pre–image $\mathbf{w}_0(1-\xi)^2 + \mathbf{w}_1 2(1-\xi)\xi + \mathbf{w}_2\,\xi^2$ of this PH quintic, to obtain the cubic polynomial $\tilde{\mathbf{w}}(\xi)$ with Bernstein coefficients

$$\tilde{\mathbf{w}}_0 = \mathbf{w}_0, \quad \tilde{\mathbf{w}}_1 = \frac{\mathbf{w}_0 + 2\,\mathbf{w}_1}{3}, \quad \tilde{\mathbf{w}}_2 = \frac{2\,\mathbf{w}_1 + \mathbf{w}_2}{3}, \quad \tilde{\mathbf{w}}_3 = \mathbf{w}_2. \quad (40)$$

Hence, we choose $\lambda = |\mathbf{w}_0|^2 = |\mathbf{w}_2|^2$ and

$$(p_1, q_1) = \frac{(\mathrm{Re}(\tilde{\mathbf{w}}_1), \mathrm{Im}(\tilde{\mathbf{w}}_1))}{\sqrt{\lambda}}, \quad (p_2, q_2) = \frac{(\mathrm{Re}(\tilde{\mathbf{w}}_2), \mathrm{Im}(\tilde{\mathbf{w}}_2))}{\sqrt{\lambda}} \quad (41)$$

as starting values to solve the system of equations (29)–(32).

Remark 2. For any values $(\mathbf{w}_0, \mathbf{w}_1, \mathbf{w}_2)$ that identify a PH quintic solution obtained from the algorithm in Appendix 1, the values $(-\mathbf{w}_0, -\mathbf{w}_1, -\mathbf{w}_2)$ also specify a solution (obtained by replacing w by $-w$ in step 3) that defines exactly the same curve. For these two solutions, the values of the quantities (40) — and hence of (41) — are opposites of each other. However, equations (30)–(32) incorporate both linear and quadratic terms in p_1, q_1, p_2, q_2 so they cannot be satisfied by both solutions. The starting values for p_1, q_1, p_2, q_2 are therefore identified by the solution that satisfies (30)–(32).

When the system of three equations in the variables λ, τ_1, τ_2 obtained by substituting (38) and (39) into (30)–(32) is employed, starting values for τ_1, τ_2 must be obtained, to supplement the known starting value for λ. Equations (38) and (39) specify straight lines in the (p_1, q_1) and (p_2, q_2) planes, and the starting values for τ_1 and τ_2 are identified by the points on those lines closest to the values (p_1, q_1) and (p_2, q_2) determined from the quintic PH curve, as identified by minimizing the expressions

$$F_1(\tau_1) = \left[\alpha_i\tau_1 - \beta_i\frac{\pi s_i}{6}\lambda - p_1\right]^2 + \left[\beta_i\tau_1 + \alpha_i\frac{\pi s_i}{6}\lambda - q_1\right]^2,$$

$$F_2(\tau_2) = \left[\alpha_f\tau_2 - \beta_f\frac{\pi s_f}{6}\lambda + p_2\right]^2 + \left[\beta_f\tau_2 + \alpha_f\frac{\pi s_f}{6}\lambda + q_2\right]^2.$$

---

[4]This problem has a closed–form solution incurring only univariate quadratic equations. For convenience, the solution procedure is briefly summarized in Appendix 1.

Equating the derivatives of these functions to zero yields the starting values

$$\hat{\tau}_1 \;=\; \alpha_i p_1 + \beta_i q_1 \,, \quad \hat{\tau}_2 \;=\; -(\alpha_f p_2 + \beta_f q_2)\,. \tag{42}$$

In this case the starting values satisfy equations (29), but not (30)–(32).

Once the good solution has been computed, u_1, v_1 and u_2, v_2 are obtained from (33) and we have $(u_0, v_0) = \sqrt{\lambda}\,(\alpha_i, \beta_i)$ and $(u_3, v_3) = \sqrt{\lambda}\,(\alpha_f, \beta_f)$. The coefficients $\mathbf{w}_k = u_k + \mathrm{i}\,v_k$ for $k = 0, \ldots, 3$ of the cubic polynomial $\mathbf{w}(\xi)$ are then known, and the PH curve approximant $\mathbf{r}(\xi)$ to the clothoid segment $s \in [\,s_i, s_f\,]$ can be constructed from expressions (5)–(7) with $m = 3$.

The starting values identified above are employed to solve equations (29)–(32) through Newton–Raphson iterations — note that these values exactly satisfy the three equations (30)–(32) but not the two equations (29). For the clothoid segments C_k, $k \geq 2$ (and subsegments thereof) these starting values yield rapid and accurate convergence to the "good" PH curve approximant. However, the segment C_1 exhibits anomalous behavior, and it is necessary to relax the condition $|\mathbf{w}_0| = |\mathbf{w}_3|$ to ensure accurate approximation of this segment and its subsegments, as described in Section 6.1.

6 Computed examples

The following examples were obtained by Newton–Raphson iterations applied to the system (29)–(32) of five equations in the variables $\lambda, p_1, q_1, p_2, q_2$ and the reduced system of three equations in the variables λ, τ_1, τ_2 determined by substituting (38)–(39) into (30)–(31), using starting values from the quintic PH curve with the same end points, tangents, and arc length as the clothoid (see Appendix 1). The two systems were observed to be similar in accuracy and efficiency. The Matlab "fsolve" function was also employed to solve the equations, and was found to yield substantially identical results.

Example 1. As a typical example, consider the monotone clothoid segment between the consecutive turning points $\mathbf{c}_2$ and $\mathbf{c}_3$ that correspond to the arc lengths $s_2 = \sqrt{2}$ and $s_3 = \sqrt{3}$. Then we have $(\alpha_i, \beta_i) = (0, 1)$ and $(\alpha_f, \beta_f) = (-1/\sqrt{2}, 1/\sqrt{2})$, with known values for $\Delta s, \Delta x, \Delta y$. The PH quintic having equal–magnitude end derivatives, and the same end points, tangents, and arc

length as this clothoid segment is identified by the complex coefficients

$$\begin{aligned}
\mathbf{w}_0 &= -0.98951702 + 0.39396136\,\mathrm{i}\,, \\
\mathbf{w}_1 &= -1.11362917 + 0.02460666\,\mathrm{i}\,, \\
\mathbf{w}_2 &= -0.97826694 - 0.42112145\,\mathrm{i}\,.
\end{aligned}$$

The PH quintic end–point curvatures, $\kappa_i = 4.501854$ and $\kappa_f = 5.356500$, are in quite good agreement with those of the clothoid segment, $\kappa_i = 4.442883$ and $\kappa_f = 5.441398$. From $\mathbf{w}_0, \mathbf{w}_1, \mathbf{w}_2$ we identify the starting values

$$\lambda = 0.32457761\,,$$

$$p_1 = -0.24353350\,, \quad q_1 = 0.98665879\,,$$

$$p_2 = -0.47923576\,, \quad q_2 = 0.88902772\,,$$

for solving the system of equations (29)–(32). This is an excellent starting approximation, and the Newton–Raphson method converges to the "good" solution with double–precision accuracy in just 4 iterations, yielding

$$\lambda = 0.31997902\,,$$

$$p_1 = -0.23693822\,, \quad q_1 = 0.99619189\,,$$

$$p_2 = -0.49495712\,, \quad q_2 = 0.90534616\,.$$

The computed coefficients of the cubic polynomial $\mathbf{w}(\xi)$ are then

$$\begin{aligned}
\mathbf{w}_0 &= -0.00000000 + 0.56566688\,\mathrm{i}\,, \quad \mathbf{w}_1 = -0.13402810 + 0.56351276\,\mathrm{i}\,, \\
\mathbf{w}_2 &= -0.27998085 + 0.51212433\,\mathrm{i}\,, \quad \mathbf{w}_3 = -0.39998689 + 0.39998689\,\mathrm{i}\,,
\end{aligned}$$

and they generate the Bézier control points

$$\begin{aligned}
\mathbf{p}_0 &= (0.52889160, 0.71397221)\,, \quad \mathbf{p}_1 = (0.48318031, 0.71397221)\,, \\
\mathbf{p}_2 &= (0.43764309, 0.70314146)\,, \quad \mathbf{p}_3 = (0.39541073, 0.68114400)\,, \\
\mathbf{p}_4 &= (0.35989888, 0.64880163)\,, \quad \mathbf{p}_5 = (0.33432109, 0.60827808)\,, \\
\mathbf{p}_6 &= (0.32105619, 0.56301641)\,, \quad \mathbf{p}_7 = (0.32105619, 0.51730512)\,.
\end{aligned}$$

The degree 7 PH curve determined by these control points has end points, tangents, and curvatures, and total arc length, in agreement with the exact clothoid to an accuracy of 14 decimal places or better.
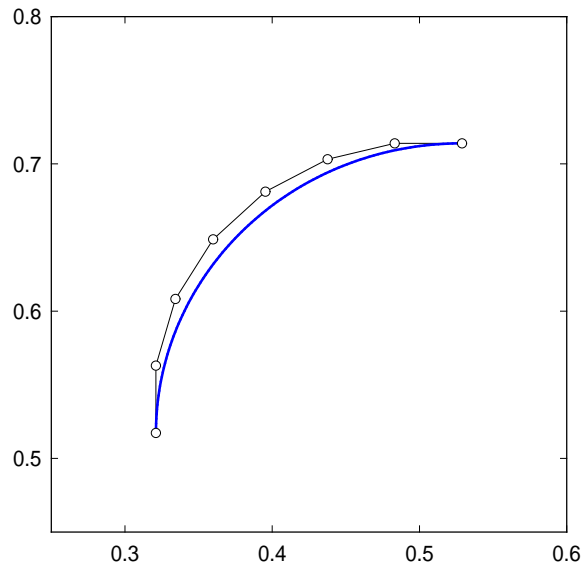
16

Figure 2: The degree 7 PH curve that matches the end points, tangents, and curvatures, and total arc length, of the clothoid segment between the turning points $\mathbf{c}_2$ and $\mathbf{c}_3$, corresponding to the arc length interval $s \in [\, s_2, s_3 \,]$.
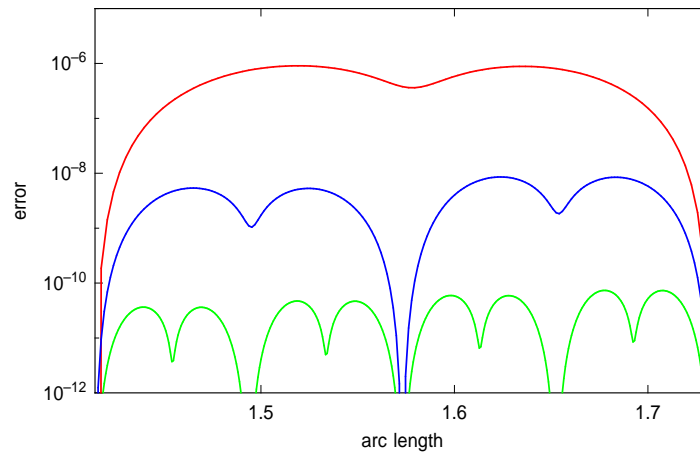

Figure 3: Variation of the error (43) of the degree 7 PH curve approximant $\mathbf{r}(\xi)$ to the clothoid segment $s \in [\, s_2, s_3 \,]$ in Figure 2, shown on a logarithmic scale (red graph). The blue and green graphs show the diminution of error achieved by dividing $\mathbf{r}(\xi)$ into two and four subsegments of equal arc length.

17

Figure 2 shows the degree 7 PH curve approximant $\mathbf{r}(\xi)$ with its Bézier control polygon. The deviation from the exact clothoid $\mathbf{c}(s) = (C(s), S(s))$ specified by the Fresnel integrals (2) for $s \in [\sqrt{2}, \sqrt{3}]$ is defined as

$$e(s) = |\mathbf{r}(\xi_*) - \mathbf{c}(s)|, \tag{43}$$

where ξ_* is the parameter value corresponding to arc length $s_* = s - s_i$ along $\mathbf{r}(\xi)$ — i.e., it is the unique real root of equation (17), which can be computed to machine precision by a few Newton–Raphson iterations

$$\xi_*^{(k)} = \xi_*^{(k-1)} - \frac{s(\xi_*^{(k-1)}) - s_*}{\sigma(\xi_*^{(k-1)})}, \quad k = 1, 2, \dots$$

from a starting approximation $\xi_*^{(0)}$. As seen in Figure 3, we have $e(s) < 10^{-6}$ along the entire curve, and the error can be further suppressed by considering smaller segments. Figure 3 shows that $e(s)$ is less than 10^{-8} and 10^{-10} when $\mathbf{r}(\xi)$ is divided into two and four subsegments, respectively. This is consistent with the known $O(h^6)$ approximation order [10] of "ordinary" cubics matching the end points, tangents, and curvatures of a given curve.

For this example, Figure 4 shows the near–linear variation of the curvature κ defined by (13) with arc length over the interval $s \in [s_2, s_3]$. The exact clothoid is characterized by the relation $\mathrm{d}\kappa/\mathrm{d}s = \pi$. In Figure 4 we plot the arc–length derivative

$$\frac{\mathrm{d}\kappa}{\mathrm{d}s} = \frac{x'y''' - x'''y' - 3\,\sigma\,(x'x'' + y'y'')\,\kappa}{\sigma^4},$$

of the curvature $\kappa = (x'y'' - x''y')/\sigma^3$ for the PH curve approximant. The variation of $\mathrm{d}\kappa/\mathrm{d}s$ lies within the narrow range $[0.9841\,\pi, 1.0065\,\pi]$.

Finally, Figure 4 also shows the the normalized parametric speed $\sigma(\xi)/\Delta s$ (which is exactly equal to 1 for a true arc–length parameterization) along the PH curve. Although the PH curve approximation scheme does not explicitly attempt to minimize variations in the parametric speed, it is seen to lie within the narrow range $\sigma(\xi)/\Delta s \in [0.9963, 1.0067]$ — indicating that $\mathbf{r}(\xi)$ quite closely approximates a true arc–length parameterization.

The accuracy with which the degree 7 PH curve approximates the clothoid properties $\kappa = \pi\,s$ and $\xi = s/\Delta s$ can be further improved by subdivision, as with the behavior of the error (43) shown in Figure 3.
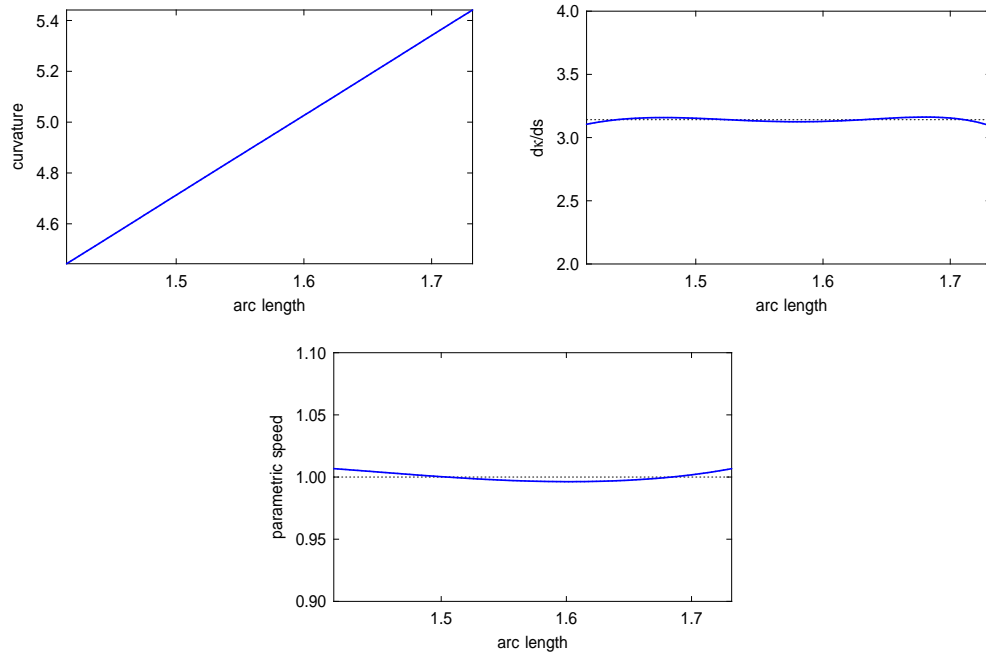
Figure 4: Variation of curvature κ (upper left), arc–length derivative $\mathrm{d}\kappa/\mathrm{d}s$ of curvature (upper right), and "normalized" parametric speed $\sigma(\xi)/\Delta s$ (lower) with arc length s along the PH curve approximant to clothoid segment C_3.

Table 1 indicates the number of Newton–Raphson iterations required for convergence to the "good" PH curve approximant of the monotone clothoid segments $s \in [\, s_{k-1}, s_k \,]$, $1 \leq k \leq 12$. Also indicated is the root–mean–square deviation of points corresponding to equal arc length along the clothoid and the degree 7 PH curve approximant, and root–mean–square deviation of the normalized parametric speed $\sigma(\xi)/\Delta s_k$ from unity: these values are based on a sampling of 101 points at uniform arc length increments along both curves.

It is evident that, for each $k \geq 2$, the monotone clothoid segments C_k are approximated with a high degree of consistency in both point–wise accuracy and in emulating arc–length parameterization. For the segments $2 \leq k \leq 12$, convergence behavior similar to that described in Example 1 was observed under subdivision into two and four subsegments. However, as can be seen in Table 1, segment C_1 is more difficult to accurately approximate by a single degree 7 PH curve, and it behaves less predictably under subdivision.

segment	iterations	e_{rms}	σ_{rms}
C_1	4	3.0337×10^{-4}	3.2916×10^{-2}
C_2	4	8.9057×10^{-7}	2.4429×10^{-3}
C_3	4	5.8428×10^{-7}	3.2644×10^{-3}
C_4	4	3.7392×10^{-7}	3.6137×10^{-3}
C_5	4	2.6200×10^{-7}	3.7602×10^{-3}
C_6	4	1.9592×10^{-7}	3.8345×10^{-3}
C_7	4	1.5340×10^{-7}	3.8772×10^{-3}
C_8	4	1.2423×10^{-7}	3.9041×10^{-3}
C_9	4	1.0324×10^{-7}	3.9220×10^{-3}
C_{10}	4	8.7542×10^{-8}	3.9345×10^{-3}
C_{11}	4	7.5456×10^{-8}	3.9437×10^{-3}
C_{12}	4	6.5915×10^{-8}	3.9506×10^{-3}

Table 1: Iterations required for convergence to machine precision of PH curve approximants to the clothoid segments $C_1, \ldots, C_{12}$. Also listed are the root–mean–square deviation of corresponding points on the clothoid segment and PH curve (e_{rms}), and of the normalized parametric speed from unity (σ_{rms}).

Remark 3. As already noted, the system of equations (29)–(32) may admit multiple real solutions. The existence of multiple interpolants to discrete data — among which the "good" solution must be identified — is a characteristic

feature of PH curves [14, 18, 26, 35]. Since the non–linear nature of equations (29)–(32) precludes a simple analysis of the number of distinct real solutions $\lambda, p_1, q_1, p_2, q_2$ for each monotone segment C_k, we investigate this empirically. To reduce the dimension of the solution space, we employ the reduced system of three equations in the variables λ, τ_1, τ_2 obtained by substituting (38)–(39) into (30)–(32). We then record the number of distinct real solutions obtained by Newton–Rapshon iterations from starting values defined by a $21 \times 21 \times 21$ grid over the domain $(\lambda, \tau_1, \tau_2) \in [\, 0, \lambda_{\max} \,] \times [\, \tau_{1,\min}, \tau_{1,\max} \,] \times [\, \tau_{2,\min}, \tau_{2,\max} \,]$, where $\lambda_{\max}$ is given by (34), and the intervals in τ_1 and τ_2 are centered on the values $\hat{\tau}_1, \hat{\tau}_2$ given by (42), and of width $4\,|\hat{\tau}_1|$ and $4\,|\hat{\tau}_2|$. For each monotone segment $C_2, \ldots, C_{12}$ exactly *four distinct real solutions* were found. However, only *two* distinct real solutions were found[5] for the segment C_1.

Figure 5 shows the four distinct PH curve interpolants to the end points, tangents, curvatures, and total arc length of the monotone clothoid segment C_3. Although all four solutions precisely match the clothoid segment data, only one (the "good" solution) approximates the clothoid segment with high accuracy. One other solution is of reasonable shape but poorer accuracy. The remaining two solutions are inconsistent with the clothoid segment shape — one has two extremely tight loops (barely visible in the plot), and the other has inflections. Table 2 quantifies this behavior in terms of the pointwise error e_{rms}, parametric speed error σ_{rms}, and deviation of the curvature derivative $\mathrm{d}\kappa/\mathrm{d}s$ from the clothoid value π. This illustrates the key role of the quintic PH curve in ensuring rapid convergence to the good solution.

solution	e_{rms}	σ_{rms}	$\mathrm{d}\kappa/\mathrm{d}s$
1	5.8428×10^{-7}	3.2644×10^{-3}	$[\, 0.9814, 1.0065 \,]\, \pi$
2	1.3921×10^{-5}	1.0853×10^{-1}	$[\, 0.6942, 2.2594 \,]\, \pi$
3	2.2574×10^{-3}	7.2976×10^{-1}	$[\, -7.1290, 5.1632 \,] \times 10^8\, \pi$
4	1.5629×10^{-2}	8.0829×10^{-1}	$[\, -1.8067, 1.3748 \,] \times 10^3\, \pi$

Table 2: Approximation quality of the four distinct PH curves interpolating the end points, tangents, curvatures, and arc length of clothoid segment C_3.

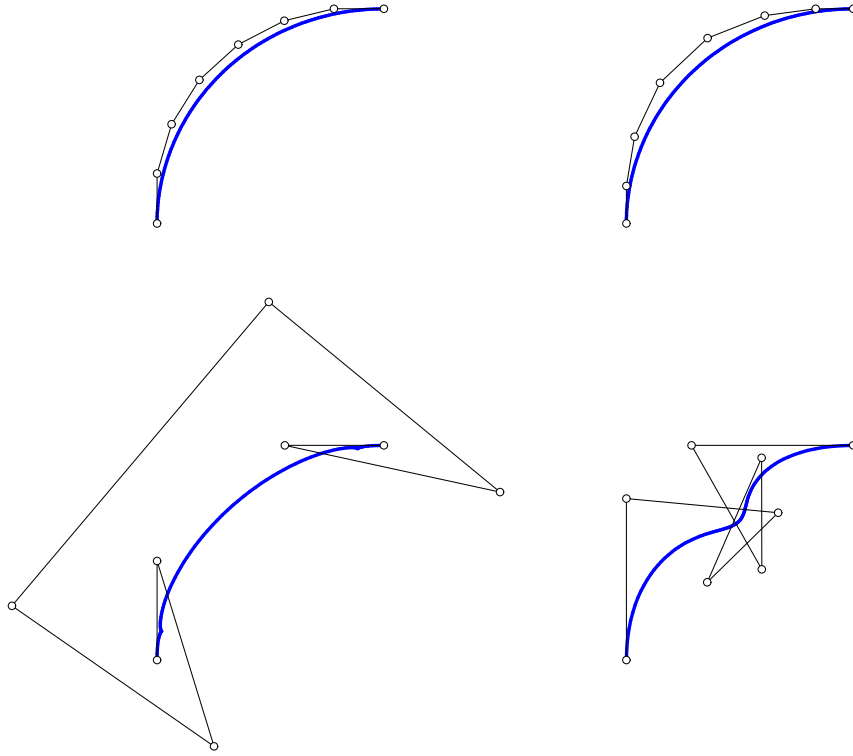[5]This remained unchanged upon doubling the resolution of the grid of starting values, and increasing its extent.

Figure 5: The distinct PH curve solutions for clothoid segment C_3: the good solution (upper left); a curve of reasonable shape but poorer accuracy (upper right); a curve with tight loops (lower left); a non–convex curve (lower right).

6.1 The monotone segment C_1

We now consider in greater detail the anomalous behavior of the approximant to clothoid segment C_1, corresponding to $s \in [0, 1]$. This example converges to machine precision in 4 iterations, but with a deviation e_{rms} significantly larger than the subsequent segments C_k, $k \geq 2$ (see Table 1). Figure 6 shows the PH curve approximant, and Figure 7 illustrates the arc–length derivative of curvature and parametric speed variation, which have more pronounced deviations than for the subsequent segments.
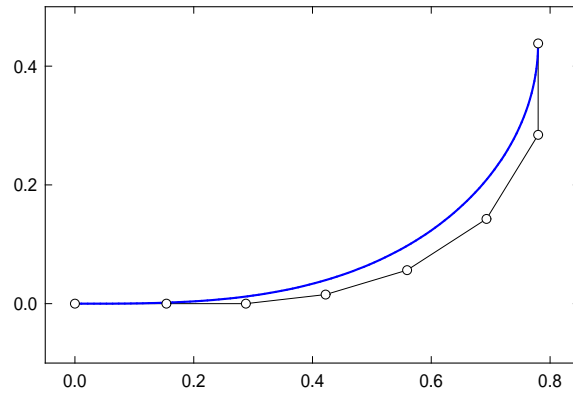

Figure 6: The degree 7 PH curve that matches the end points, tangents, and curvatures, and total arc length, of the monotone clothoid segment between turning points $\mathbf{c}_0$ and $\mathbf{c}_1$, corresponding to the arc length interval $s \in [0, 1]$.

Example 2. Table 3 lists results obtained when C_1 is split into two, four, and eight subsegments of equal arc length, where "×" indicates cases that failed to converge or converged to a solution other than the "good" solution. It is seen that convergence problems are associated with the arc–length interval $s \in [0.50, 0.75]$, for which the starting values appear to be near a singularity of the system (29)–(32). For all other subsegments of C_1, rapid convergence and excellent accuracy of the PH curve approximant are obtained.

The problematic C_1 subsegments were also investigated using the `Matlab` "Fsolve" function. For these subsegments, Fsolve was observed to terminate upon reaching the maximum allowed number of iterations, since the Jacobian matrix becomes nearly singular. The solutions thus obtained appear to define monotone curvature segments, although they are of relatively poor accuracy as approximations of the corresponding clothoid segments.
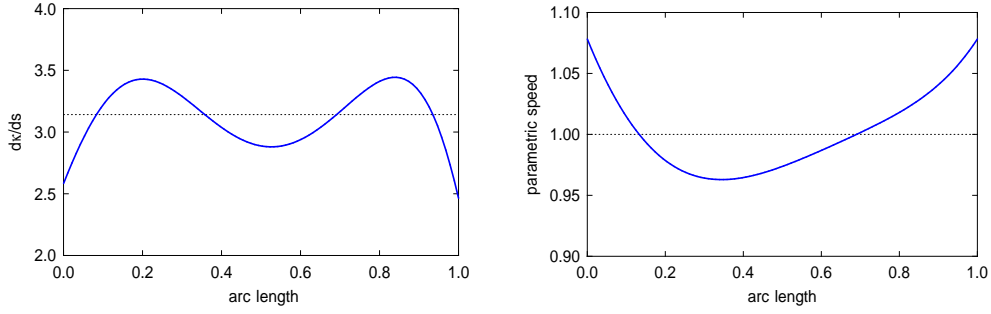
23

Figure 7: Left: arc–length derivative of curvature $\mathrm{d}\kappa/\mathrm{d}s$ for the degree 7 PH curve approximation to the clothoid segment $s \in [\,0,1\,]$ in Figure 6. Right: the "normalized" parametric speed $\sigma(\xi)/\Delta s$ for the PH curve approximant.

arc length	iterations	e_{rms}	σ_{rms}
$[\,0.000, 0.500\,]$	3	1.0703×10^{-6}	1.4260×10^{-3}
$[\,0.500, 1.000\,]$	$\times$	——	——
$[\,0.000, 0.250\,]$	2	7.9335×10^{-9}	8.7648×10^{-5}
$[\,0.250, 0.500\,]$	3	9.4164×10^{-9}	9.7905×10^{-4}
$[\,0.500, 0.750\,]$	$\times$	——	——
$[\,0.750, 1.000\,]$	6	4.0017×10^{-8}	4.6025×10^{-3}
$[\,0.000, 0.125\,]$	2	6.1790×10^{-11}	5.4728×10^{-6}
$[\,0.125, 0.250\,]$	3	5.8250×10^{-11}	5.6681×10^{-5}
$[\,0.250, 0.375\,]$	3	6.4322×10^{-11}	1.6453×10^{-4}
$[\,0.375, 0.500\,]$	3	8.8487×10^{-11}	3.6535×10^{-4}
$[\,0.500, 0.625\,]$	5	1.9390×10^{-10}	9.8652×10^{-4}
$[\,0.625, 0.750\,]$	$\times$	——	——
$[\,0.750, 0.875\,]$	$\times$	——	——
$[\,0.875, 1.000\,]$	5	1.1020×10^{-10}	5.1284×10^{-4}

Table 3: Convergence behavior for the monotone segment C_1 subdivided into two, four, and eight subsegments of equal arc length. An "$\times$" indicates failure to converge, or convergence to a solution other than the "good" solution.

It is evident that segment C_1 (and its subsegments) pose greater difficulty in identifying "good" PH curve approximants, subject to all of the imposed conditions. To address this, we relax the requirement $|\mathbf{r}'(0)| = |\mathbf{r}'(1)| = \lambda$ of equal end–point parametric speeds, and instead set[6] $|\mathbf{r}'(0)| = \lambda$, $|\mathbf{r}'(1)| = \eta\,\lambda$ where η is a free parameter that can be exploited to identify and optimize good PH curve approximants. Upon writing $(u_0, v_0) = \sqrt{\lambda}\,(\alpha_i, \beta_i)$, $(u_1, v_1) = \sqrt{\lambda}\,(p_1, q_1)$, $(u_2, v_2) = \sqrt{\eta\,\lambda}\,(p_2, q_2)$, $(u_3, v_3) = \sqrt{\eta\,\lambda}\,(\alpha_f, \beta_f)$, each instance of $p_2, q_2, \alpha_f, \beta_f$ in equations (30)–(32) is replaced with $\sqrt{\eta}\,p_2, \sqrt{\eta}\,q_2, \sqrt{\eta}\,\alpha_f, \sqrt{\eta}\,\beta_f$ and λ in (39) is replaced with $\eta\,\lambda$, but (38) remains unchanged.

Since large disparities in the end–derivative magnitudes are unlikely to yield curves of good shape quality, it is advisable to restrict η to values close to 1, e.g., $\eta \in [\,0.5, 1.5\,]$. A simple bisection method can be employed to find optimum η values that yield rapid convergence, with excellent accuracy of the clothoid approximant. This approach is best suited for off–line computation, allowing the PH curve to be imported into a CAD system through its control points and the coefficients of the pre–image polynomial (4) once it has been identified. Alternatively, the "reverse engineering" methodology described in [15] can be used to determine the coefficients of (4) from the control points.

Example 3. Consider the C_1 subsegment $s \in [\,0.5, 1.0\,]$ (for which no good solution exists when $|\mathbf{r}'(0)| = |\mathbf{r}'(1)|$). As η varies, either two or four distinct solutions are observed, and among values that admit a "good" solution, $\eta = 0.8986$ is observed to yield the smallest deviation from the exact clothoid, with $e_{\mathrm{rms}} = 6.9235 \times 10^{-8}$. Figure 8 shows the resulting PH curve, together with the variation of the error (43), the normalized parametric speed, and the arc–length derivative of curvature $\mathrm{d}\kappa/\mathrm{d}s$.

The entire segment C_1 was also revisited using the above approach, with $\eta = 0.7932$ being found to yield the optimum error value $e_{\mathrm{max}} = 1.4068 \times 10^{-6}$, significantly smaller than the value indicated in Table 1 that corresponds to $\eta = 1$, but the variation of the parametric speed ($\sigma_{\mathrm{rms}} = 7.2508 \times 10^{-2}$) is somewhat higher. The arc–length derivative of curvature $\mathrm{d}\kappa/\mathrm{d}s$ was found to vary within the relatively narrow range $[\,0.9914, 1.0033\,]\,\pi$. This optimized PH curve approximant to the clothoid segment C_1 is preferable when positional accuracy is more important than uniformity of the parametric speed.

---

[6]This affects the uniformity of parameterization, but does not alter interpolation of the end–points, tangents, and curvatures, and the total arc length.
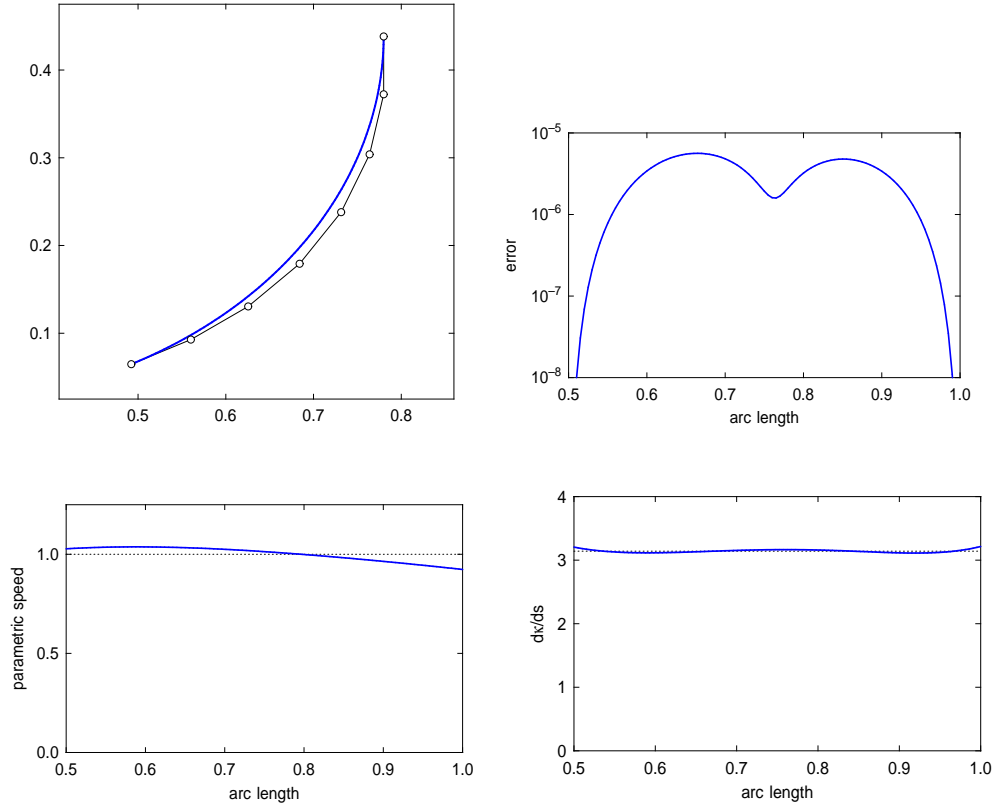
Figure 8: Approximation of the clothoid subsegment $s \in [\frac{1}{2}, 1]$ using unequal end–point parametric speeds $|\mathbf{r}'(1)|/|\mathbf{r}'(0)| = \eta$ with $\eta = 0.8986$ (upper left). Also shown are graphs of the pointwise error (upper right), parametric speed variation (lower left), and arc–length derivative of curvature (lower right).

7 Closure

Precise control over curvature variation is a basic requirement in the design of planar free–form curves. Beyond the trivial instances of a constant curvature (lines and circles), the most fundamental case is a linear variation of curvature with arc length. This property identifies the *clothoid*, a transcendental curve defined in terms of the Fresnel integrals whose evaluation is computationally expensive and susceptible to error amplification in floating–point arithmetic.

The present study demonstrates that clothoid segments can be accurately approximated by degree 7 PH curves that interpolate the segment end points, tangents, and curvatures, and also match their total arc lengths. In addition to closely emulating the linear relation between curvature and arc length, the approximants are observed to have a near–constant parametric speed — i.e., the curve parameter is very nearly proportional to the arc length.

The focus herein was on approximation of *monotone* clothoid segments. By concatenating these approximations (or subsegments thereof), extended piecewise clothoid approximations with G^2 continuity can be obtained. The construction is based on solving a system of five algebraic equations in five real variables through Newton–Raphson iteration, with initial values derived from a closed–form solution for a quintic PH curve that matches the segment end points and tangents (but not curvatures), and the total arc length. With these values, convergence to machine precision is typically observed in just 4 iterations, and the approximation accuracy can be greatly enhanced through subdivision of the monotone clothoid segments into smaller pieces.

Appendix 2 enumerates (to 8 decimal places) the Bernstein coefficients of the cubic pre–image polynomials for the degree 7 PH curve approximants to the first 12 monotone clothoid segments. These data allow the PH curve clothoid approximants to be directly employed in applications without having to implement the numerical procedures described herein.

Acknowledgements

Scientifico, which F. Pelosi and M. L. Sampoli are members of.

Appendix 1: construction of PH quintic

We briefly summarize the algorithm [14] to compute a planar PH quintic with given end points, end tangents, and total arc length, that is used to generate starting values for iterative solution of the system of equations (29)–(32).

input: initial/final points $\mathbf{p}_i, \mathbf{p}_f$, tangents $\mathbf{t}_i, \mathbf{t}_f$, and arc length S.

1. convert the input data to canonical form by setting $\ell = |\mathbf{p}_f - \mathbf{p}_i|$ and $\alpha = \arg(\mathbf{p}_f - \mathbf{p}_i)$, and (a) subtracting $\mathbf{p}_i$ from $\mathbf{p}_i, \mathbf{p}_f$; (b) dividing $\mathbf{p}_f$ by $\ell \exp(i\,\alpha)$; (c) dividing $\mathbf{t}_i, \mathbf{t}_f$ by $\exp(i\,\alpha)$; and (d) dividing S by ℓ;

2. set $\theta_m = \frac{1}{2}(\theta_i + \theta_f)$, $\delta\theta = \frac{1}{2}(\theta_f - \theta_i)$ and assign $(c_i, s_i) = (\cos\frac{1}{2}\theta_i, \sin\frac{1}{2}\theta_i)$, and $(c_f, s_f) = (\cos\frac{1}{2}\theta_f, \sin\frac{1}{2}\theta_f)$;

3. set $z = -(a_1 + \sqrt{a_1^2 - 4\,a_2 a_0})/2a_2$ and $w = \sqrt{z}$, where $a_2 = 2\sin^2\delta\theta$, $a_1 = 6\,[\,(\cos\delta\theta - 3)S + (3\cos\delta\theta - 1)\cos\theta_m\,]$, $a_0 = 36\,(S^2 - 1)$;

4. with $p(z) = 60(S+1) - (15c_i^2 + 15c_f^2 - 10c_ic_f)z$ and $q(z) = 60(S-1) - (15s_i^2 + 15s_f^2 - 10s_is_f)z$, determine whether like or unlike signs $\mu = \pm 1$ and $\nu = \pm 1$ satisfy
$$\mu\nu \sqrt{p(z)}\sqrt{q(z)} = 5(c_is_f + c_fs_i - 3c_is_i - 3c_fs_f)z\,;$$

5. for the two sign combinations of μ, ν thus identified, compute
$$u = \frac{-3(c_i + c_f)w + \mu\sqrt{p(z)}}{4} \quad\text{and}\quad v = \frac{-3(s_i + s_f)w + \nu\sqrt{q(z)}}{4}\,;$$

6. for the two sets of u, v, w values thus obtained, form the complex values
$$\mathbf{w}_0 = w\exp(i\tfrac{1}{2}\theta_i)\,,\quad \mathbf{w}_1 = u + i\,v\,,\quad \mathbf{w}_2 = w\exp(i\tfrac{1}{2}\theta_f)\,;$$

7. identify the good solution, with the least value of $|2\,\mathbf{w}_1 - (\mathbf{w}_0 + \mathbf{w}_2)|^2$;

8. map the canonical–form good solution to the original coordinates by multiplying $\mathbf{w}_0, \mathbf{w}_1, \mathbf{w}_2$ with $\sqrt{\ell}\,\exp(i\,\tfrac{1}{2}\alpha)$ and obtain the control points from (5) and (7) with $m = 2$ and $\mathbf{p}_0 = \mathbf{p}_i$.

output: planar PH quintic PH $\mathbf{r}(\xi)$ with $\mathbf{r}(0) = \mathbf{p}_i$, $\mathbf{r}(1) = \mathbf{p}_f$, $\mathbf{r}'(0) = w^2\mathbf{t}_0$, $\mathbf{r}'(1) = w^2\mathbf{t}_1$ and the prescribed arc length S.

Appendix 2: degree 7 PH curve coefficients

The coefficients of the cubic complex polynomial (4) are listed consecutively for the degree 7 PH curve approximants to the clothoid segments $C_1, \ldots, C_{12}$. The values for segment C_1 correspond to the optimum parameter value $\eta = 0.7932$ identified in Example 3, and for all the other segments they correspond to the case of identical end–point parametric speeds. These coefficients suffice to construct the PH curve approximants, and determine all their properties.

$$\mathbf{w}_0 = 1.06637917 + 0.00000000\,i\,, \quad \mathbf{w}_1 = 1.01606069 + 0.00000000\,i\,,$$
$$\mathbf{w}_2 = 0.99420510 + 0.35986432\,i\,, \quad \mathbf{w}_3 = 0.67156493 + 0.67156493\,i\,.$$

$$\mathbf{w}_0 = 0.45558728 + 0.45558728\,i\,, \quad \mathbf{w}_1 = 0.35823093 + 0.55628026\,i\,,$$
$$\mathbf{w}_2 = 0.19804933 + 0.63932971\,i\,, \quad \mathbf{w}_3 = 0.00000000 + 0.64429771\,i\,.$$

$$\mathbf{w}_0 = 0.00000000 + 0.56566688\,i\,, \quad \mathbf{w}_1 = -0.13402810 + 0.56351276\,i\,,$$
$$\mathbf{w}_2 = -0.27998085 + 0.51212433\,i\,, \quad \mathbf{w}_3 = -0.39998689 + 0.39998689\,i\,.$$

$$\mathbf{w}_0 = -0.36744956 + 0.36744956\,i\,, \quad \mathbf{w}_1 = -0.45529351 + 0.27531841\,i\,,$$
$$\mathbf{w}_2 = -0.51445155 + 0.14694906\,i\,, \quad \mathbf{w}_3 = -0.51965215 + 0.00000000\,i\,.$$

$$\mathbf{w}_0 = -0.48785924 + 0.00000000\,i\,, \quad \mathbf{w}_1 = -0.48456766 - 0.12159402\,i\,,$$
$$\mathbf{w}_2 = -0.43766348 - 0.24540645\,i\,, \quad \mathbf{w}_3 = -0.34496858 - 0.34496858\,i\,.$$

$$\mathbf{w}_0 = -0.32803844 - 0.32803844\,i\,, \quad \mathbf{w}_1 = -0.24299857 - 0.40831569\,i\,,$$
$$\mathbf{w}_2 = -0.12805409 - 0.45933923\,i\,, \quad \mathbf{w}_3 = 0.00000000 - 0.46391641\,i\,.$$

$$\mathbf{w}_0 = 0.00000000 - 0.44490088\,i\,, \quad \mathbf{w}_1 = 0.11294423 - 0.44152650\,i\,,$$
$$\mathbf{w}_2 = 0.22525226 - 0.39777741\,i\,, \quad \mathbf{w}_3 = 0.31459243 - 0.31459243\,i\,.$$

$$\mathbf{w}_0 = 0.30351971 - 0.30351971\,i\,, \quad \mathbf{w}_1 = 0.37862052 - 0.22367881\,i\,,$$
$$\mathbf{w}_2 = 0.42507399 - 0.11712492\,i\,, \quad \mathbf{w}_3 = 0.42924169 + 0.00000000\,i\,.$$

$$\mathbf{w}_0 = 0.41600272 + 0.00000000\,\mathrm{i}\,, \quad \mathbf{w}_1 = 0.41268645 + 0.10661839\,\mathrm{i}\,,$$
$$\mathbf{w}_2 = 0.37128453 + 0.21135695\,\mathrm{i}\,, \quad \mathbf{w}_3 = 0.29415834 + 0.29415834\,\mathrm{i}\,.$$

$$\mathbf{w}_0 = 0.28608399 + 0.28608399\,\mathrm{i}\,, \quad \mathbf{w}_1 = 0.21020983 + 0.35732604\,\mathrm{i}\,,$$
$$\mathbf{w}_2 = 0.10965395 + 0.40070283\,\mathrm{i}\,, \quad \mathbf{w}_3 = 0.00000000 + 0.40458386\,\mathrm{i}\,.$$

$$\mathbf{w}_0 = 0.00000000 + 0.39457884\,\mathrm{i}\,, \quad \mathbf{w}_1 = -0.10171851 + 0.39134607\,\mathrm{i}\,,$$
$$\mathbf{w}_2 = -0.20090940 + 0.35178233\,\mathrm{i}\,, \quad \mathbf{w}_3 = -0.27900937 + 0.27900937\,\mathrm{i}\,.$$

$$\mathbf{w}_0 = -0.27273156 + 0.27273156\,\mathrm{i}\,, \quad \mathbf{w}_1 = -0.34093387 + 0.20001760\,\mathrm{i}\,,$$
$$\mathbf{w}_2 = -0.38203412 + 0.10407356\,\mathrm{i}\,, \quad \mathbf{w}_3 = -0.38570066 + 0.00000000\,\mathrm{i}\,.$$

References

[1] M. Alazah, S. N. Chandler–Wilde, and S. La Porte (2014), Computing Fresnel integrals via modified trapezium rules, *Numer. Math.* **128**, 635–661.

[2] Y. Boersma (1969), Computation of Fresnel integrals, *Math. Comp.* **14**, 380.

[3] A. Atmosudiro, A. Verl, A. Lechler, and G. Schwarz (2017), A clothoid based real–time interpolation concept for path smoothing, Proceedings, 3rd IEEE International Conference on Control, Automation, and Robotics, 41–46.

[4] K. G. Baass (1984), The use of clothoid templates in highway design, *Transport. Forum* **1**, 47–52.

[5] E. Bertolazzi and M. Frego (2018), On the G^2 interpolation problem with clothoids, *J. Comput. Appl. Math.* **341**, 99–116.

[6] M. Brezak and I. Petrović (2014), Real–time approximation of clothoids with bounded error for path planning applications, *IEEE Trans. Robot.* **30**, 507–515.

[7] Y. Chen, Y. Cai, J. Zheng, and D. Thalmann (2017), Accurate and efficient approximation of clothoids using Bézier curves for path planning, *IEEE Trans. Robot.* **33**, 1242–1247.

[8] H. I. Choi and H. P. Moon (2008), Weierstrass–type approximation theorems with Pythagorean hodograph curves, *Comput. Aided Geom. Design* **25**, 305–319.

[9] S. D. Conte and C. de Boor (1980), *Elementary Numerical Analysis: An Algorithmic Approach*, McGraw–Hill, New York.

[10] C. de Boor, K. Höllig, and M. Sabin (1987), High accuracy geometric Hermite interpolation, *Comput. Aided Geom. Design* **4**, 269–278.

[11] R. T. Farouki (1994), The conformal map $z \rightarrow z^2$ of the hodograph plane, *Comput. Aided Geom. Design* **11**, 363–390.

[12] R. T. Farouki (1997), Pythagorean–hodograph quintic transition curves of monotone curvature, *Comput. Aided Design* **29**, 601–606.

[13] R. T. Farouki (2008), *Pythagorean–Hodograph Curves: Algebra and Geometry Inseparable*, Springer, Berlin.

[14] R. T. Farouki (2016), Construction of G^1 planar Hermite interpolants with prescribed arc lengths, *Comput. Aided Geom. Design* **46**, 64–75.

[15] R. T. Farouki, C. Giannelli, and A. Sestini (2015), Identification and "reverse engineering" of Pythagorean–hodograph curves, *Comput. Aided Geom. Design* **34**, 21–36.

[16] R. T. Farouki, J. Manjunathaiah, and S. Jee (1998), Design of rational cam profiles with Pythagorean–hodograph curves, *Mech. Mach. Theory* **33**, 669–682.

[17] R. T. Farouki, J. Manjunathaiah, D. Nicholas, G.–F. Yuan, and S. Jee (1998), Variable feedrate CNC interpolators for constant material removal rates along Pythagorean–hodograph curves, *Comput. Aided Design* **30**, 631–640.

[18] R. T. Farouki and C. A. Neff (1995), Hermite interpolation by Pythagorean hodograph quintics, *Math. Comp.* **64**, 1589–1609.

31

[19] R. T. Farouki, F. Pelosi, and M. L. Sampoli (2019), Optimization of corner blending curves, *Comput. Aided Design* **117**, article 102739.

[20] R. T. Farouki and S. Shah (1996), Real–time CNC interpolators for Pythagorean–hodograph curves, *Comput. Aided Geom. Design* **13**, 583–600.

[21] S. Fleury, P. Souères, J–P. Laumond, and R. Chatila (1995), Primitives for smoothing mobile robot trajectories, *IEEE Trans. Robot. Autom.* **11**, 441–448.

[22] Z. Habib and M. Sakai (2007), On PH quintic spirals joining two circles with one circle inside the other, *Comput. Aided Design* **39**, 125–132.

[23] Z. Habib and M. Sakai (2007), G^2 Pythagorean hodograph quintic transition between two circles with shape control, *Comput. Aided Geom. Design* **24**, 252–266.

[24] P. Hartman (1957), The highway spiral for combining curves of different radii, *Trans. Amer. Soc. Civil Eng.* **22**, 389–409.

[25] M. A. Heald (1985), Rational approximations for the Fresnel integrals, *Math. Comp.* **44**, 459–461.

[26] B. Jüttler (2001), Hermite interpolation by Pythagorean hodograph curves of degree seven, *Math. Comp.* **70**, 1089–1111.

[27] E. Kreyszig (1959), *Differential Geometry*, University of Toronto Press.

[28] P. F. Lima, M. Trincavelli, J. Martensson, and B. Wahlberg (2015), Clothoid–based model predictive control for autonomous driving, Proceedings, 2015 European Control Conference, 2983–2990.

[29] D. S. Meek and R. S. D. Thomas (1991), A guided clothoid spline, *Comput. Aided Geom. Design* **8**, 163–174.

[30] D. S. Meek and D. J. Walton (1989), The use of Cornu spirals in drawing planar curves of controlled curvature, *J. Comput. Appl. Math.* **25**, 69–78.

[31] D. S. Meek and D. J. Walton (1992), Clothoid spline transition spirals, *Math. Comp.* **59**, 117–133.

[32] D. S. Meek and D. J. Walton (2004), An arc spline approximation to a clothoid, *J. Comput. Appl. Math.* **170**, 59–77.

[33] K. D. Mielenz (1997), Computation of Fresnel integrals, *J. Res. Natl. Inst. Stand. Technol.* **102**, 380.

[34] K. D. Mielenz (2000), Computation of Fresnel integrals. II, *J. Res. Natl. Inst. Stand. Technol.* **105**, 589–590.

[35] H. P. Moon, R. T. Farouki, and H. I. Choi (2001), Construction and shape analysis of PH quintic Hermite interpolants, *Comput. Aided Geom. Design* **18**, 93–115.

[36] S. Narayan (2014), Approximating Cornu spirals by arc splines, *J. Comput. Appl. Math.* **255**, 789–804.

[37] M. Nitulescu and M. Ivanescu (2020), Connections for path planning in mobile robotics, in Advances in Service and Industrial Robotics (K. Berns and D. Görges, eds.), 259–266, Springer, Berlin.

[38] A. W. Nutbourne, P. M. McLellan, and R. M. L. Kensit (1972), Curvature profiles for plane curves, *Comput. Aided Design* **4**, 176–184.

[39] M. Raković, S. Savić, J. Santos–Victor, M. Nikolić, and B. Borovac (2019), Human–inspired online path planning and biped walking realization in unknown environment, *Front. Neurorobot.* **13**, DOI: 10.3389/fnbot.2019.00036.

[40] J. Sanchez–Reyes and J. M. Chacon (2003), Polynomial approximation to clothoids via *s*–power series, *Comput. Aided Design* **35**, 1305–1313.

[41] A. Shahzadeh, A. Khosravi, T. Robinette, and S. Nahavandi (2018), Smooth path planning using biclothoid fillets for high speed CNC machines, *Int. J. Mach. Tools Manufac.* **132**, 36–49.

[42] M. Shanmugavel, A. Tsourdos, B. White, and R. Zibowski (2010), Cooperative path planning of multiple UAVs using Dubins paths with clothoid arcs, *Contr. Eng. Pract.* **18**, 1084–1092.

[43] Y–F. Tsai, R. T. Farouki, and B. Feldman (2001), Performance analysis of CNC interpolators for time–dependent feedrates along PH curves, *Comput. Aided Geom. Design* **18**, 245–265.

[44] G. Vanegas, L. Armesto, and V. Girbés (2019), Clothoid–based three–dimensional curve for attitude planning, *J. Guid. Contr. Dyn.* **42**, 1886–1898.

[45] W. Van Snyder (1993), Algorithm 723 Fresnel integrals, *ACM Trans. Math. Software* **19**, 452–456.

[46] M. E. Vázquez–Méndez and G. Casal (2016), Clothoid computation: a simple and efficient numerical algorithm, *J. Survey Eng.* **142**, Article 04016005.

[47] D. J. Walton and D. S. Meek (2002), Planar G^2 transition with a fair Pythagorean hodograph quintic curve, *J. Comput. Appl. Math.* **138**, 109–126.

[48] D. J. Walton and D. S. Meek (2007), G^2 curve design with a pair of Pythagorean hodograph quintic spiral segments, *Comput. Aided Geom. Design* **24**, 267–285.